RANS computations of tip vortex cavitation

2015 J. Phys.: Conf. Ser. 656 012183

(http://iopscience.iop.org/1742-6596/656/1/012183)

RANS computations of tip vortex cavitation

Jean Decaix[1], Guillaume Balarac[2], Matthieu Dreyer[3], Mohamed Farhat[3], Cécile Münch[1]

[1], University of Applied Sciences and Arts, Western Switzerland, 47 Route du Rawyl, 1950 Sion, Switzerland
[2], Univ. Grenoble Alpes, LEGI, F-38000 Grenoble, France, CNRS, LEGI, F-38000 Grenoble, France
[3], Ecole Polytechnique Fédérale de Lausanne, Laboratory for Hydraulic Machines, 33 Bis Av. De Cour, 1007 Lausanne, Switzerland

E-mail: jean.decaix@hevs.ch

Abstract. The present study is related to the development of the tip vortex cavitation in Kaplan turbines. The investigation is carried out on a simplified test case consisting of a NACA0009 blade with a gap between the blade tip and the side wall. Computations with and without cavitation are performed using a RANS modelling and a transport equation for the liquid volume fraction. Compared with experimental data, the RANS computations turn out to be able to capture accurately the development of the tip vortex. The simulations have also highlighted the influence of cavitation on the tip vortex trajectory.

1. Introduction

Confined tip vortices develop in the gap between a blade tip of a finite span and a side wall due to the pressure difference between the blade pressure and suction sides. Close to the leading edge, this pressure difference generates a leakage jet that rolls up to form the so-called tip-leakage vortex. The leakage jet and the vortex are influenced by the gap width as shown experimentally [1, 2] and numerically [3, 4]. Furthermore, the tip-leakage vortex promotes the cavitation inception [5] due to the low pressure reached in the vortex core. Regarding Kaplan turbines, the damages depend on the strength and the trajectory of the vortex. The prediction of these two characteristics are a challenging task for the computations.
The present paper deals with a numerical investigation of the confined tip-leakage vortex. The test case is a NACA0009 blade mounted in a rectangular channel with a gap between the blade tip and the side wall. Computations are carried out for one particular gap width, with and without cavitation. The results are analysed and compared with experimental data [2].

2. Experimental test case

The hydrofoil used in both the numerical and experimental cases is a blunt trailing edge NACA0009 [2] with a chord length $c = 100$ mm and a maximum thickness of 9.9 mm. It is mounted in the EPFL high-speed cavitation tunnel in a rectangular channel section of 150 mm $\times$ 150 mm $\times$ 750 mm . The foil incidence is $i = 10°$. The gap τ between the blade tip and the side wall is set to $\tau/c = 0.1$. The inlet velocity is $u_{inlet} = 10.2\ m.s^{-1}$, which leads to a Reynolds number based on the chord length $Re_c = 10^6$. The cavitation number σ_u is computed using the

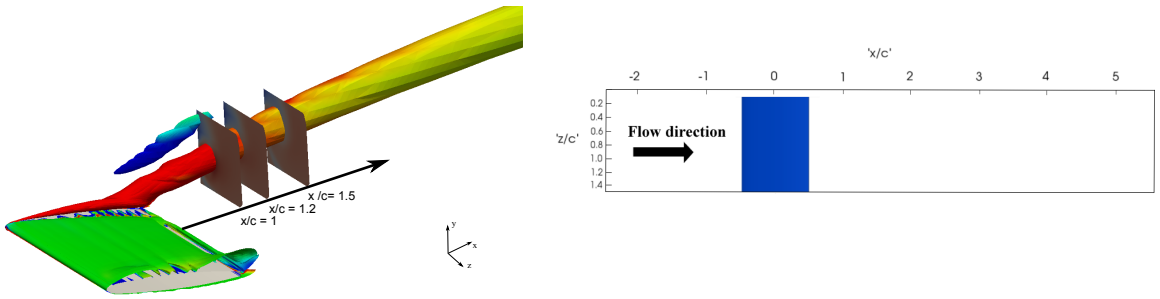

Figure 1. Left: position of the experimental measurement sections with the tip vortex highlighted by an iso-surface of the Q-criterion. Right: Computational domain (top view).

pressure reference located upstream of the leading edge:

$$\sigma_u = \frac{p_{ref} - p_{sat}}{\frac{1}{2}\rho u_{inlet}^2} = 2.01 \tag{1}$$

With :

$$p_{ref} = 107'000\,Pa \quad p_{sat} = 2'300\,Pa \quad \rho = 1'000\,kgm^{-3} \tag{2}$$

For the non-cavitating case, the available experimental data are the velocity fields at three cross sections downstream of the trailing edge (see figure 1 left). For the cavitating case, only flow visualisations are performed from the side of the test section.

3. Numerical set up

The computations are performed on a domain similar to the experimental test section except for the channel length, which extends two chords upstream of the leading edge and five chords downstream of the trailing edge (see figure 1 right). The OpenFOAM 2.1.0 software is used to solve the RANS equations. Turbulence is modelled with the $k-\omega$ SST model. Cavitation is taken into account by solving an additional transport equation for the liquid volume fraction defined by:

$$\frac{\partial \alpha_L}{\partial t} + (\vec{u} \cdot \nabla)\,\alpha_L = m_c + m_v \tag{3}$$

Where :

$$m_c = \frac{\rho}{\rho_L \rho_V} C_c \frac{\rho_V}{t_\infty} \alpha_{Llim}^2 \frac{\max(p - p_{sat}\,;\,0)}{\max(p - p_{sat}\,;\,0.01\,p_{sat})} \tag{4}$$

$$m_v = \frac{\rho}{\rho_L \rho_V} C_v \frac{\rho_V}{\frac{1}{2}\rho_L U_\infty^2 t_\infty} \min(p - p_{sat}\,;\,p_0) \tag{5}$$

The parameters are set to: $C_v = 800$, $C_c = 500$, $U_\infty = u_{inlet} = 10.2$ ms^{-1} and $t_\infty = 0.005$ s.
A structured mesh containing 2 million of nodes is generated with 30 nodes along the spanwise direction in the gap. The inlet velocity profile is set by using the velocity profile provided by a RANS computation on a computational domain twice longer. The pressure level is set at the experimental probe section upstream of the blade, whereas a zero gradient pressure condition is imposed at the outlet.

Table 1. Dimensionless position of the vortex core.

x/c	Experiment	Non-cavitating RANS computation	Absolute error (%)
1.0	y/c = 0.141	y/c = 0.132	6.4
	z/c = 0.120	z/c = 0.107	11.0
1.2	y/c = 0.183	y/c = 0.179	2.2
	z/c = 0.132	z/c = 0.122	7.6
1.5	y/c = 0.303	y/c = 0.217	28.4
	z/c = 0.160	z/c = 0.149	6.9

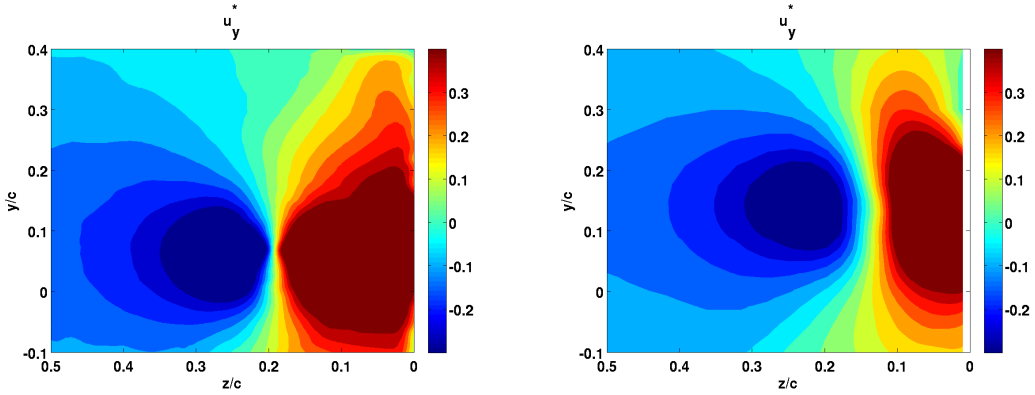

Figure 2. Dimensionless pitchwise velocity component at the first cross section located at $x/c = 1$. Experiment (left) and non-cavitating RANS computation (right).

4. Results

4.1. Non-cavitating case

Figure 2 compares the experimental and computed contours of the dimensionless pitchwise component of the velocity field ($u_y^* = u_y/u_{inlet}$) one chord downstream the trailing edge. The computation agrees with the experimental both regarding the position of the contours and the magnitude of the velocity. The main difference occurs at the vortex centre where the spanwise gradient is smoother for the computation. Table 1 gathers the dimensionless pitchwise and spanwise position of the vortex core determined by the location of the maximum of axial vorticity. Except for the pitchwise position at the last section, the position of the vortex is captured with less than approximately 10% of error by the computation. Such an error represents less than 2 millimetres, which is approximately the mesh cell size. Therefore, the position of the vortex core downstream of the blade is considered to be fairly captured by the computation.

4.2. Cavitating case

To compute the cavitating case, the cavitation number has been decreased to $\sigma_u = 1.3$ instead of the experimental value $\sigma_u = 2.1$. Indeed, as the RANS computation is not able to fully resolve the vortex core, the pressure drop at the vortex centre is underestimated compared to the experiment. The pressure level in the computation is thus decreased to obtain an amount of cavitation in the vortex core similar to the experimental one. Figure 3 shows the iso-surface of the liquid volume fraction provided by the computation and an instantaneous experimental picture of the cavitating tip vortex. The position and the size of the tip vortex cavitation are well captured by the computation. Downstream of the blade, due to the mesh resolution, cavitation cannot be maintained. The iso-surface of the dimensionless Q-criterion is displayed on figure 4

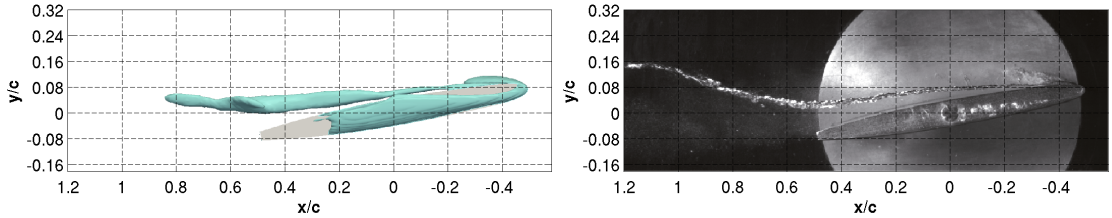

Figure 3. Iso-surface of the mean liquid volume fraction $\alpha_L = 0.9$ provided by the cavitating RANS computation (left) and instantaneous experimental picture (right).

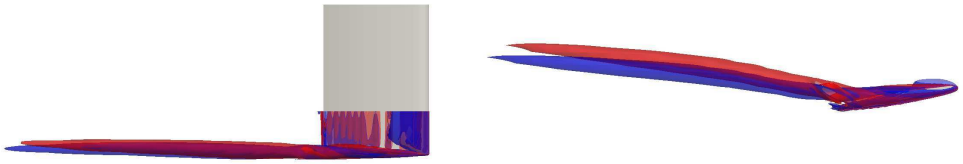

Figure 4. Iso-surface of the dimensionless Q-criterion. Top view (left) and side view (right). Red: non cavitating case. Blue: cavitating case.

both for the non cavitating and the cavitating cases. It is observed that the tip vortex trajectory is influenced by the cavitation. In absence of cavitation, the tip vortex moves upward and to the centre of the channel at it travels downstream. In presence of cavitation, the tip vortex moves upward more slowly and remains close to the side wall. This difference can be explained by the detachment of the boundary layer at the leading edge of the blade (not shown here) due to a thin layer of cavitation. The detachment is followed by a recirculation zone on the suction side that leads the tip vortex to move towards the blade. Furthermore, the detachment provokes a large wake downstream of the blade that confines the tip vortex close to the side wall.

5. Conclusion

The one-phase RANS computation is able to capture the tip vortex trajectory and the velocity field with reasonable accuracy compared to the experiment. By decreasing the pressure level in the channel, cavitation occurs in the vortex core in agreement with the experimental observations. It is shown that the tip vortex moves closer to the suction side of the blade and the side wall, which have to be taken into account regarding the cavitation erosion risk.

Acknowledgements

The authors are very grateful to the Competence Center in Energy and Mobility (CCEM), Swisselectric Research and the foundation The Ark through the program The Ark Energy for their financial support.

References

[1] Muthanna C and Devenport W J 2004 *AIAA Journal* **42** 2320–2331
[2] Dreyer M, Decaix J, Münch C and Farhat M 2014 *Experiment in Fluids* **55**
[3] You D, Wang M, Moin P and Mittal R 2006 *Physics of Fluids* **18**
[4] Decaix J, Balarac G, Dreyer M, Farhat M and Münch C 2015 *Journal of Turbulence* **16** 309–341
[5] Arndt R E A 2002 *Annual Review of Fluid Mechanics* **34** 143–175